

The bulk Higgs in the Deformed RS Model

F. Mahmoudi^{a,b,1}, N. Manglani^{c,d}, K. Sridhar^e^a*Univ Lyon, Univ Lyon 1, CNRS/IN2P3, Institut de Physique Nucléaire de Lyon UMR5822,
F-69622 Villeurbanne, France*^b*Theoretical Physics Department, CERN, CH-1211 Geneva 23, Switzerland*^c*Department of Physics, University of Mumbai, Kalina, Mumbai 400098, India*^d*Shah and Anchor Kutchhi Engineering College, Mumbai 400088, India*^e*Department of Theoretical Physics, Tata Institute of Fundamental Research, Homi Bhabha Road, Colaba,
Mumbai 400 005, India*

Abstract

Electroweak precision tests allow for lighter Kaluza-Klein (KK) Higgs modes in the deformed Randall-Sundrum (RS) model than in models with custodial symmetry. The first KK mode of the Higgs (h_1) in such a model could have a mass as low as 900 GeV. In this paper, we study the production of h_1 and its subsequent decay to a $t\bar{t}$ pair at the Large Hadron Collider (LHC), in the context of the deformed RS model. We have performed a hadron-level Monte Carlo simulation of the signal and the relevant Standard Model background. We present strategies to effectively suppress the huge SM background and provide a signal that is tractable at the future runs of the LHC.

Keywords: Warped 5D model, Hierarchy problem, deformed metric, Higgs.

1. Introduction

One of the most appealing solutions to the large hierarchy between the Planck scale and the electroweak (EW) scale is provided by the Randall-Sundrum (RS) Model [1]. The RS model is a five-dimensional (5D) model with a warped geometry given by the following metric:

$$ds^2 = e^{-2A(y)} \eta_{\mu\nu} dx^\mu dx^\nu + dy^2, \quad (1)$$

¹Also Institut Universitaire de France, 103 boulevard Saint-Michel, 75005 Paris, France.

Email addresses: nazila@cern.ch (F. Mahmoudi), namrata.manglani@sakec.ac.in (N. Manglani), sridhar@theory.tifr.res.in (K. Sridhar)

where, $A(y)$ is called the warp factor. The fifth dimension is compactified on an S^1/Z^2 orbifold of radius R and, located at the orbifold fixed points, $y = 0, \pi R$ are two 3-branes: the UV and the IR brane, respectively. In the original RS model (RS1), all the Standard Model fields along with the Higgs are localised on the IR brane with only the gravitons being UV-localised. There is essentially only one mass scale to begin with, viz., the Planck scale M_p but scales associated with the IR-localised fields like the electroweak vacuum expectation value, are naturally warped down and a stable solution to the Planck-weak hierarchy results. However, in such a model even other scales that ought to be naturally large, such as the ones that suppress proton decay or flavour-changing neutral currents or provide the desirably small neutrino masses, are warped down. To avoid such issues and with the subsequent realisation that only the Higgs need be IR-localised to address hierarchy, a new class of RS models in which the Standard Model fields are allowed to propagate in the bulk were developed [2–8]. Such bulk models provide us a framework within which to confront experimental observations more realistically. For instance, localising fermions at different points in the bulk provides a tractable approach to Yukawa hierarchy [9–13].

In fact, even the Higgs field need not be exactly localised on the IR brane: the solution to the gauge-hierarchy problem requires that the Higgs be only close to it. Localising the Higgs in the bulk close to the IR brane is sufficient to solve the hierarchy problem, so it is not mandatory to fix it on the IR brane [14]. With a bulk Higgs the mass bounds on the KK gauge boson (m_{KK}) reduces from 12 TeV to 7.2 TeV, i.e. by a factor of $\sqrt{3}$ [15]. Even in this light the phenomenological studies of the Higgs first KK mode are very few and have not got their due attention as compared to other SM field KK excitations.

The bulk RS models are severely constrained by the oblique S and T parameters. The constraints from the S parameter are weakened by localising fermions in the bulk but those coming from the T parameter need more serious consideration. Two different bulk models have been proposed to address this issue:

- The first, referred to as the custodial model, invokes a bulk local symmetry ($SU(3)_c \times SU(2)_L \times SU(2)_R \times U(1)_y$) which, in a manner reminiscent of the global custodial symmetry of the SM, ameliorates the fit to the measured T parameter [16, 17]. The bound on the lightest m_{KK} comes down to about 3 TeV in such models [18, 19]. Due to the larger gauge symmetry of this model, the model has a rich spectrum of new particles. Another issue to contend with in such models is the non-universal correction to the $Z \rightarrow b\bar{b}$ vertex induced by the fact that in order to get the magnitude of the top quark mass right in bulk models, the $(t, b)_L$ doublet cannot be localised too far away from the IR brane. In custodial models, this is done by embedding the $(t, b)_L$ doublet in an $SU(2)_L \times SU(2)_R$ bidoublet with a special choice of left- and right-quantum numbers. The bidoublet contains exotic charge $\pm 5/3$ fermions.
- The same problem can be solved in the deformed RS model, without an additional symmetry. In this model, we assume a bulk Higgs i.e. a Higgs not on the IR brane but close to it and introduce an additional scalar field. Due to this extra field, warping of the fifth dimension is strongly modified near the IR brane, while it behaves as pure AdS near the UV brane. This is done using soft wall metrics and a naked singularity

generated beyond the IR brane by this scalar field. Proximity of the IR brane to the singularity determines the strength of the modification. The deformation of the metric tends to localise the gauge KK modes closer to the IR brane than in the normal RS model and with the Higgs zero mode localised further out in the bulk its overlap with the gauge KK modes is reduced. This relaxes the electroweak constraints considerably [19, 20].

In addition the $Z \rightarrow b\bar{b}$ partial width and flavour observables also provide stringent constraints on the gauge KK mass. However even after taking these into account, lower bounds on $m_{KK} \sim \mathcal{O}(1 - 2 \text{ TeV})$ are obtained [21] in a reasonably significant part of the parameter space of this model, making it interesting from the LHC perspective.

Given that the deformed RS model is a viable alternative to the actively investigated custodial RS model, it is worthwhile to also subject the deformed RS model to a more critical scrutiny, specially from the point of view of collider searches. A couple of studies of collider signals in the deformed model have been published [22, 23], but, other collider signals in the deformed model are crying out for attention.

In this paper, we study the production of the first KK mode of Higgs within the framework of deformed RS model. A similar study for the same process within the custodial RS model was published by us earlier [24]. However, the significantly lower mass range available for the first KK mode of the Higgs in the deformed RS model and the much smaller production cross sections as compared to custodial RS model makes the collider analysis more challenging. Not only do the lower cross sections pose a challenge but at the lower mass end the Standard Model backgrounds also turn out to be a very serious problem. It is to address these challenges that we have to alter the analysis from the previously studied custodial case [24].

The paper is structured as follows: In Section 2 we provide a brief introduction to the deformed RS model along with a brief description of the constraints. In Section 3 we give a detailed explanation regarding the signal and background simulations and the strategies used to suppress the background effectively. In Section 4 we summarise the results.

2. Bulk Higgs in Deformed RS Model

The action for a bulk Higgs and other scalar fields (ϕ) in a 5D theory is given by [14]:

$$S_5 = \int d^4x dy \sqrt{-g} \left[-|D_M H|^2 - \frac{1}{2}|D_M \phi|^2 - V(H, \phi) - \Sigma_\alpha (-1)^\alpha 2\lambda^\alpha(H, \phi) \delta(y - y_\alpha) \right], \quad (2)$$

where $\lambda^\alpha (\alpha = 0, 1)$ are the brane potentials for the UV and the IR branes respectively, which are of the form $\lambda^0(\phi_0, H) = M_0|H|^2$ and $-\lambda^1(\phi_1, H) = -M_1|H|^2 + \gamma|H|^4$. Here ϕ_α is the vacuum expectation value of the field ϕ at the two boundaries of the fifth dimension $y = y_\alpha$.

The $V(H, \phi)$ is the 5D scalar potential having a quadratic mass term with the coefficient $M(\phi)$ and H is the 5D Higgs field having the notation:

$$H(x^\mu, y) = \frac{1}{\sqrt{2}} \begin{bmatrix} 0 \\ h(y) + \xi(x^\mu, y) \end{bmatrix},$$

3

where $h(y)$ is the Higgs background and $\xi(x^\mu, y)$ can be expanded as a series of the Higgs KK modes. For a small Higgs mass, we can assume that the vacuum expectation value (vev) is almost entirely carried by the zero mode (h_0), hence the zero mode profile is the same as the vev profile.

The differential equations for the profiles of $h(y)$ and $\xi(y)$ are obtained by varying the 5D action of the scalar fields given in Eq. (2)

$$h''(y) - 4A'(y)h'(y) - \frac{\partial V}{\partial h} = 0 , \quad (3)$$

with the boundary conditions

$$\frac{h'(y_\alpha)}{h(y_\alpha)} = \frac{\partial \lambda^\alpha(h)}{\partial h} |_{y=y_\alpha} . \quad (4)$$

Similarly, for $\xi(y)$ we have

$$\xi''(y) - 4A'(y)\xi'(y) - \frac{\partial^2 V}{\partial h^2} \xi(y) + m_n^2 e^{2A} \xi(y) = 0 , \quad (5)$$

with the boundary conditions

$$\frac{\xi'(y_\alpha)}{\xi(y_\alpha)} = \frac{\partial^2 \lambda^\alpha(h)}{\partial h^2} |_{y=y_\alpha} . \quad (6)$$

After simplifying the above differential equations, we can obtain the solutions for the profiles of h_0 and h_1 .

The profile equations for the h_0 and fermion zero modes ($t_0^{L,R}$) as given in Refs. [21, 23] are

$$\begin{aligned} f_0^h &= N_0^h e^{aky - A(y)} , \\ f_0^{t_{L,R}} &= N_0^{t_{L,R}} e^{(0.5 \mp c)A(y)} . \end{aligned} \quad (7)$$

Using these profile equations we fix the value of the fermion mass parameter (c) by fitting the top quark mass [19]. We fit the 5D Yukawa (y_5) to the SM Yukawa (y_4) using these profiles ($y_4 = y_5 \int_0^{y_1} f_0^h f_0^{t_L} f_0^{t_R} dy$) by multiplying the 5D Yukawa with the profile overlap integral for the profiles of the zero-mode Higgs to the zero-mode left handed top quark and the zero-mode right handed top quark. The coupling modifier (y_{100}/y_4) for the h_1 coupling to the zero-mode top quarks is given as the ratio of the profile overlap for KK Higgs first mode with the top quarks to the profile overlap of KK Higgs zero mode with the top quarks ($y_{100} = y_4 \times \frac{\int_0^{y_1} f_1^h f_0^{t_L} f_0^{t_R} dy}{\int_0^{y_1} f_0^h f_0^{t_L} f_0^{t_R} dy}$).

The main ingredient of the deformed RS model [20, 25] is the modified metric given in Eq. (1), where the warp factor $A(y) = ky$ for the custodial RS model and for the deformed RS model is

$$A(y) = ky - \frac{1}{\nu^2} \text{Log}(1 - \frac{y}{y_s}) . \quad (8)$$

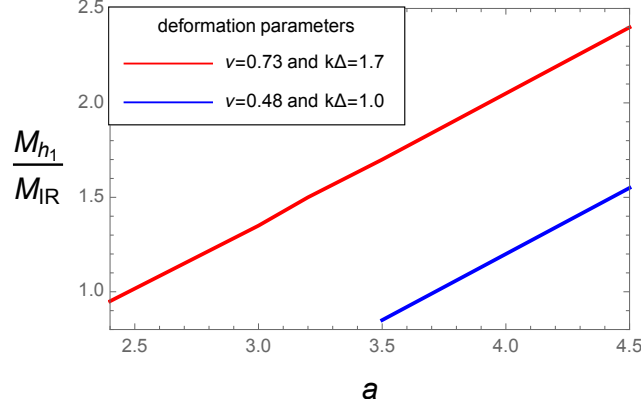


Figure 1: Variation of the KK Higgs mass for its first mode (M_{h_1}) in terms of the IR scale (M_{IR}) with respect to a parameter for two sets of deformed model parameters.

Here y_s denotes the position of the singularity which is at a distance of Δ beyond the IR brane (y_1) along the fifth dimension such that $y_s = y_1 + \Delta$. The parameter ν defines the extent of deformity, $\nu \rightarrow \infty$ being the limit in which this model is like the normal RS model without deformation. The parameter Δ is the measure of proximity of the IR brane to the singularity. Thus we have ν and Δ as free parameters of the model. The y_1 value is fixed using the constraint $A(y_1) = 36$, which is required to solve the hierarchy problem. To keep the perturbativity in the 5D theory under control we keep $M_5 L_1 \geq 1$, where M_5 is the 5D Planck scale ($M_p^2 = M_5^3 \int e^{-2A(y)} dy$) and L_1 is the curvature radius at the IR brane. Since $kL_1 = \frac{\nu^2 k \Delta}{\sqrt{1 - 2\nu^2/5 + 2\nu^2 k \Delta + \nu^4 (k \Delta)^2}}$, if we choose $kL_1 < 1$ we get a parameter set for deformed model that departs from AdS. A smaller value of kL_1 implies larger deformation. If we select $kL_1 \geq 0.2$ the hierarchy between M_5 and k can be restricted from growing too large. The fine tuning parameter $\delta \equiv |f(y_1)| \lesssim \mathcal{O}(1)$ implies that the Higgs solution is free of fine-tuning, where $f(y)$ is defined in the Eq. (6.5) in Ref. [20]. For this model the coefficient of the quadratic mass term in the scalar potential is $M(\phi) = k^2 [a(a-4) - 4ae^{\nu\phi/\sqrt{6}}]$, where a is the Higgs bulk mass parameter.

The solution to the gauge hierarchy problem demands that the Higgs field zero mode should be localised on/close to the IR brane. This implies that $a \geq a_0$, for the RS model without deformation $a_0 = 2$. In case of the deformed RS model, we choose $a_0 = 2A(y_1)/ky_1$ as given in Ref. [21]. The mass of the KK Higgs mode m_n depends on the IR scale ($M_{IR} = k e^{-A(y_1)}$) and a . The variation of the mass of the KK Higgs first mode (M_{h_1}) in terms of M_{IR} with respect to the parameter a for two sets of deformation parameters can be seen in Figure 1. Thus we show that the lower value of the a parameter for a given set of deformation parameters can be more interesting for the deformed RS model from the point of view of LHC phenomenology. The parameter space that we consider in the following is $\nu = 0.48$ and $k\Delta = 1$ and $a = 3.2$ [20].

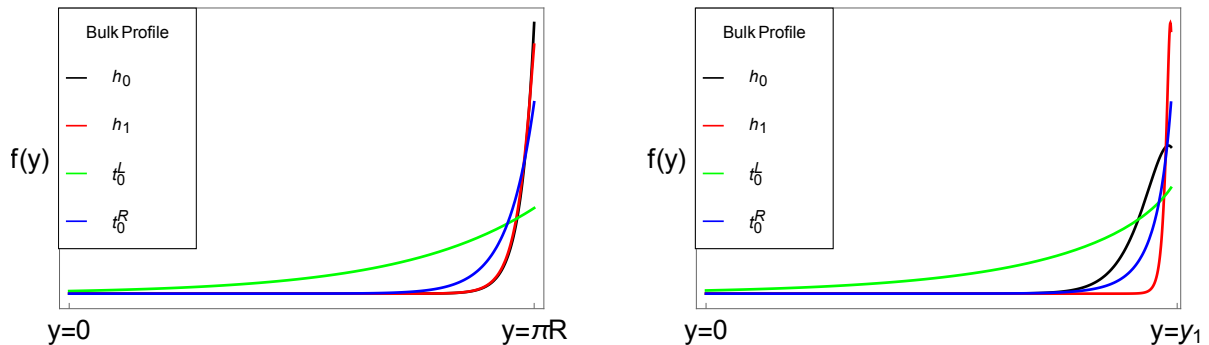


Figure 2: Profiles for the first KK mode of Higgs (red), zero-mode of Higgs (black), zero-mode of t^R (blue) and zero-mode of t^L (green) for the custodial RS model in the left and the deformed RS model in the right.

In Figure 2, we have the plotted profiles f_0^{tL} , f_0^{tR} , f_1^h and f_0^h for the custodial and deformed RS model. We observe that the f_0^h profile is less IR localised whereas the f_1^h is more IR localised in the deformed model. This reduces the profile overlap of h_1 with the t_L and t_R in the deformed model, resulting into smaller couplings which makes the effective cross section in the deformed model smaller as compared to the custodial case for the same M_{h_1} . Hence a separate search strategy is required for the deformed case. Moreover, the softer couplings and the resulting tiny cross sections imply that the existing constraints from direct searches at the LHC have little impact on this model.

3. Signal and background simulation

The signal is characterised by a bulk Higgs (h_1), which is the Kaluza Klein first mode of the Higgs boson decaying to a pair of boosted top quarks in the context of deformed RS model. For this model the coupling of h_1 to the weak bosons vanishes at leading order due to the orthogonality condition for profiles of h_1 and h_0 . The production cross section for the h_1 in association with a top quark pair is very small. Hence, gluon-gluon fusion is the main process for the production of h_1 . The coupling of h_1 to the top quark pair is nearly equal to the SM top Yukawa coupling. We probe signals with $M_{h_1} > 800$ GeV. At this mass the top decay channel is open and dominant. Thus the signal topology that we are interested to study is as follows:

$$p p (g g) \rightarrow h_1 \rightarrow t \bar{t} \quad (9)$$

The model files for h_1 were generated using FEYNRULES [26] taking into account the effective coupling of h_1 to a pair of gluons via a top quark loop. The parton-level amplitudes for the signal were generated using MADGRAPH [27] at 14 TeV centre of mass energy using parton distribution function NNLO1 [28], and showering was done in PYTHIA 8 [29]. The most dominant backgrounds for our signal are $t\bar{t}$ and QCD. Events for the $t\bar{t}$ background and the QCD background have been generated directly in PYTHIA 8. To generate the background events with larger statistics, we choose phase space cuts specified by $\hat{p}_T > 300$ GeV and

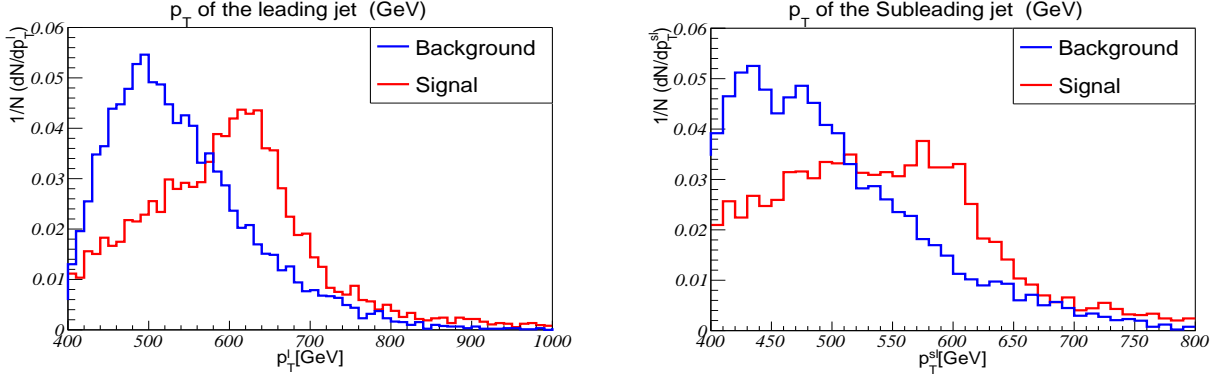


Figure 3: Normalised distribution of the p_T for leading jet (left) and subleading jet (right). The red distribution represents the signal and the blue one represents the $t\bar{t}$ background for $M_{h_1} = 1300$ GeV.

$\hat{m} \in (M_{h_1} - 300 \text{ GeV}, M_{h_1} + 300 \text{ GeV})$ for the mass range of 900 GeV to 1000 GeV, while $\hat{p}_T > 400 \text{ GeV}$ and $\hat{m} \in (M_{h_1} - 300 \text{ GeV}, M_{h_1} + 300 \text{ GeV})$ are chosen for the mass range of 1100 GeV to 1300 GeV, where the hat represents the outgoing parton system.

The signal is characterised by a pair of top quarks which come from the decay of massive h_1 and they tend to be boosted, with their transverse momentum in the range of 200 GeV to 500 GeV. Such a boost will ensure that the top decay products will lie in a single hemisphere. So, we have reconstructed fat jets from final state partons employing FASTJET [30, 31] and using the Cambridge Aachen (C-A) algorithm [32, 33] for clustering by setting the jet radius parameter $R = 1.5$. We accept only those jets which satisfy $|\eta| < 2.7$ and $p_T > 300 \text{ GeV}$.

We are interested in hadronic decays of the top quark, therefore we select events which have no leptons that satisfy $p_T > 25 \text{ GeV}$ and $|\eta| < 2.5$. Once we have a hadronic decay of both the top quarks, we need the event to be characterised with two fat jets and each of them should satisfy $|\eta| < 2.7$ and $p_T > 300 \text{ GeV}$. These two fat jets are then considered as an input for the HEPTopTagger [34, 35]. This is the most effective top tagger in the momentum range of our interest. Once both the leading and subleading jets pass the HEPTopTagger, the event is selected for further analysis.

The use of HEPTopTagger helps in reducing the QCD background whereas a mass dependent p_T cut on the leading jet and the subleading jet helps in curbing both the QCD and SM $t\bar{t}$ backgrounds. The p_T cuts for the leading and subleading jets from $M_{h_1} = 1300 \text{ GeV}$ can be explained by plots shown in Figure 3. The SM $t\bar{t}$ background largely peaks at comparatively lower transverse momentum. It is thus brought under control using a p_T cut on the leading jet ($p_T^l > 580 \text{ GeV}$) and the subleading jet ($p_T^{sl} > 540 \text{ GeV}$). The QCD background is huge, specially for the invariant mass range of our interest it is very difficult to control it with a p_T cut alone. We bring it down by using b -tagging inside the fat jet tagged as a top-jet using HEPTopTagger.

A fat jet which is tagged as a top-jet has three main subjets, two of them reconstruct the W boson mass and the remaining one is a b -like subjet. We calculate the ΔR between this

b -like subjet and the b -quark for both the leading and subleading top-tagged fat jets. Events that give a $\Delta R < 0.1$ (tight b -tag) for both the leading and subleading top-tagged jets, are referred as double b -tag events. Selecting such events after the use of **HEPTopTagger** helps to tame the QCD background. We have also taken into account the mistagging probabilities of c -quarks (20%) and light quarks(1%) for a b -tagging efficiency of 0.7 [36].

We present two sets of cuts, one suited for the lower mass of the h_1 and the other one for the higher mass of the h_1 , as shown in Table 1.

M_{h_1} (GeV)	Cuts	Signal (fb)	$t\bar{t}$ (fb)	QCD (fb)
900	2 fat jets with $p_{Tmin} = 300$ GeV	101.22	4730.86	6338534.63
	2 top-tagged jets	10.72	553.77	3641.83
	$p_T^l > 380$ GeV and $p_T^{sl} > 360$ GeV	7.28	264.62	2446.48
	b -tagging for both the jets	3.09	118.12	0
	$900 \text{ GeV} < m_{t\bar{t}} < 1000 \text{ GeV}$	1.49	35.28	0
1300	2 fat jets with $p_{Tmin} = 300$ GeV	13.66	1036.8	1120199.03
	2 top-tagged jets	1.55	137.05	833.46
	$p_T^l > 580$ GeV and $p_T^{sl} > 540$ GeV	0.69	30.78	302.16
	b -tagging for both the jets	0.32	15.71	0
	$1280 \text{ GeV} < m_{t\bar{t}} < 1400 \text{ GeV}$	0.16	3.24	0

Table 1: *Cut flow table for two values of the KK Higgs mass.*

Finally we demand that the invariant mass of the $t\bar{t}$ pair lies within a window close to the h_1 mass. We find that due to the ISR (Initial State Radiation) the peak of the invariant mass gets smeared towards higher $m_{t\bar{t}}$ as shown in Figure 4. We find the effect of ISR decreasing as the h_1 mass increases.

We find from Figure 5 and Table 2 that with the choice of the cuts given in Table 1 we can probe the h_1 of mass 900 GeV with the luminosity of 397 fb^{-1} but for higher masses such as 1300 GeV we require a luminosity of 3166 fb^{-1} .

M_{h_1} (GeV)	Luminosity in fb^{-1} for 5σ result	Luminosity in fb^{-1} for 3σ result
900	397	143
1000	400	144
1100	739	266
1200	1477	531
1300	3166	1139

Table 2: *Integrated luminosity in fb^{-1} for 5σ and 3σ sensitivities.*

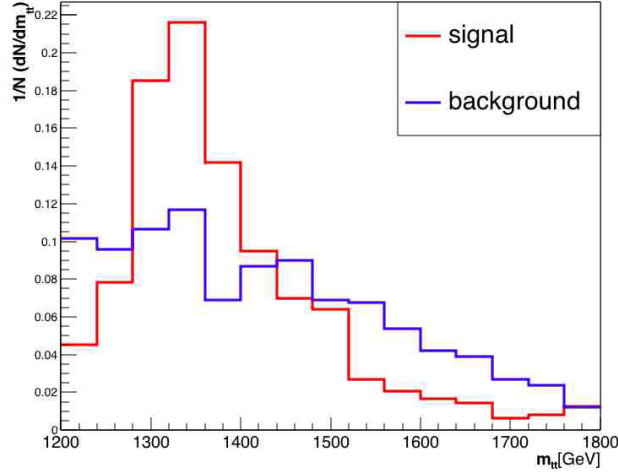


Figure 4: Normalised distributions of the invariant mass (m_{tt}) of the leading jet and subleading jet. The red distribution represents the signal and the blue one represents the $t\bar{t}$ background for $M_{h_1} = 1300$ GeV.

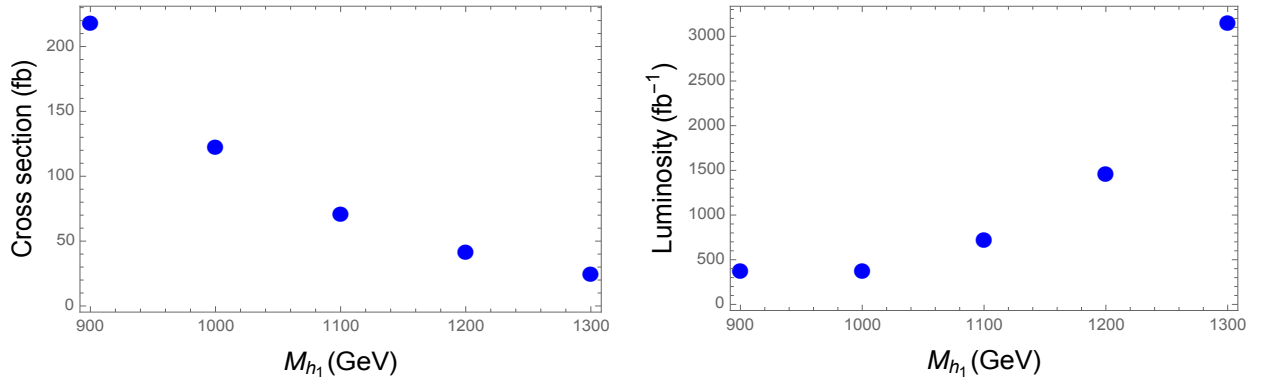


Figure 5: The effective cross section for the first mode of the KK Higgs in the deformed RS model is in the left, and the reach of luminosity at the LHC in the right.

4. Conclusion

The first KK mode of the Higgs (h_1) in the deformed RS model could be as light as 900 GeV for a choice of deformed model parameters, a , ν and Δ that can solve the hierarchy problem and be consistent with electroweak precision tests.

For such a value of KK-mass the cross section is sizeable, inspite of the small couplings in this model. However, one has to also contend with a huge SM background, to address which, we propose a new search strategy.

We start by clustering final particles into fat jets and tag them as top-jets using the HEPTopTagger. This is followed by a b -tagging which demands that the b quark be very

close to the b -like subjet inside the top-jet. This helps us to deal with the QCD background very effectively.

Our study shows that using the set of cuts that we propose, h_1 of mass 900 GeV could be probed at the LHC with a luminosity below 400 fb^{-1} . As the h_1 mass increases the cross section drops further and the required luminosity rises. Higher masses of the h_1 would need a more refined analysis or the HL-LHC.

5. Acknowledgements

N.M and K.S. would like to acknowledge the support of the CNRS LIA (Laboratoire International Associé) THEP (Theoretical High Energy Physics) and the INFRE-HEPNET (IndoFrench Network on High Energy Physics) of CEFIPRA/IFCPAR (Indo-French Centre for the Promotion of Advanced Research). N.M. would like to thank Abhishek Iyer for discussions and the Department of Theoretical Physics, TIFR for computational resources. N.M. would also like to gratefully acknowledge hospitality during her visit to IPN Lyon while this work was in progress. The authors would like to acknowledge the contributions of Ushoshi Maitra to the initial stages of this work.

References

- [1] L. Randall and R. Sundrum, *A Large mass hierarchy from a small extra dimension*, *Phys. Rev. Lett.* **83** (1999) 3370–3373, [[hep-ph/9905221](#)].
- [2] S. Raychaudhuri and K. Sridhar, *Particle Physics of Brane Worlds and Extra Dimensions*. Cambridge University Press, 2016.
- [3] T. Gherghetta, *TASI Lectures on a Holographic View of Beyond the Standard Model Physics*, *Physics of the Large and the Small, Proceedings of the Theoretical Advanced Study Institute in Elementary Particle Physics, - TASI 2009* (eds. C. Csaki and S. Dodelson) (2010) [[arXiv:1008.2570](#)].
- [4] H. Davoudiasl, J. L. Hewett, and T. G. Rizzo, *Bulk gauge fields in the Randall-Sundrum model*, *Phys. Lett.* **B473** (2000) 43–49, [[hep-ph/9911262](#)].
- [5] T. Gherghetta and A. Pomarol, *Bulk fields and supersymmetry in a slice of AdS*, *Nucl. Phys.* **B586** (2000) 141–162, [[hep-ph/0003129](#)].
- [6] A. Pomarol, *Gauge bosons in a five-dimensional theory with localized gravity*, *Phys. Lett.* **B486** (2000) 153–157, [[hep-ph/9911294](#)].
- [7] Y. Grossman and M. Neubert, *Neutrino masses and mixings in nonfactorizable geometry*, *Phys. Lett.* **B474** (2000) 361–371, [[hep-ph/9912408](#)].
- [8] S. Chang, J. Hisano, H. Nakano, N. Okada, and M. Yamaguchi, *Bulk standard model in the Randall-Sundrum background*, *Phys. Rev.* **D62** (2000) 084025, [[hep-ph/9912498](#)].
- [9] S. Casagrande, F. Goertz, U. Haisch, M. Neubert, and T. Pfoh, *Flavor Physics in the Randall-Sundrum Model: I. Theoretical Setup and Electroweak Precision Tests*, *JHEP* **0810** (2008) 094, [[arXiv:0807.4937](#)].
- [10] S. J. Huber, *Flavor violation and warped geometry*, *Nucl. Phys.* **B666** (2003) 269–288, [[hep-ph/0303183](#)].
- [11] M. Bauer, S. Casagrande, U. Haisch, and M. Neubert, *Flavor Physics in the Randall-Sundrum Model: II. Tree-Level Weak-Interaction Processes*, *JHEP* **1009** (2010) 017, [[arXiv:0912.1625](#)].
- [12] S. J. Huber and Q. Shafi, *Fermion masses, mixings and proton decay in a Randall-Sundrum model*, *Phys. Lett.* **B498** (2001) 256–262, [[hep-ph/0010195](#)].
- [13] K. Agashe, G. Perez, and A. Soni, *Flavor structure of warped extra dimension models*, *Phys. Rev.* **D71** (2005) 016002, [[hep-ph/0408134](#)].

- [14] M. Quiros, *Higgs Bosons in Extra Dimensions*, *Mod. Phys. Lett.* **A30** (2015), no. 15 1540012, [[arXiv:1311.2824](#)].
- [15] J. A. Cabrer, G. von Gersdorff, and M. Quiros, *Warped 5D Standard Model Consistent with EWPT*, *Fortsch. Phys.* **59** (2011) 1135–1138, [[arXiv:1104.5253](#)].
- [16] K. Agashe, A. Delgado, M. J. May, and R. Sundrum, *RS1, custodial isospin and precision tests*, *JHEP* **0308** (2003) 050, [[hep-ph/0308036](#)].
- [17] K. Agashe, R. Contino, L. Da Rold, and A. Pomarol, *A Custodial symmetry for Zb anti-b*, *Phys. Lett.* **B641** (2006) 62–66, [[hep-ph/0605341](#)].
- [18] H. Davoudiasl, S. Gopalakrishna, E. Ponton, and J. Santiago, *Warped 5-Dimensional Models: Phenomenological Status and Experimental Prospects*, *New J. Phys.* **12** (2010) 075011, [[arXiv:0908.1968](#)].
- [19] A. M. Iyer, K. Sridhar, and S. K. Vempati, *Bulk Randall-Sundrum models, electroweak precision tests, and the 125 GeV Higgs*, *Phys. Rev.* **D93** (2016), no. 7 075008, [[arXiv:1502.06206](#)].
- [20] J. A. Cabrer, G. von Gersdorff, and M. Quiros, *Suppressing Electroweak Precision Observables in 5D Warped Models*, *JHEP* **05** (2011) 083, [[arXiv:1103.1388](#)].
- [21] J. A. Cabrer, G. von Gersdorff, and M. Quiros, *Flavor Phenomenology in General 5D Warped Spaces*, *JHEP* **01** (2012) 033, [[arXiv:1110.3324](#)].
- [22] A. M. Iyer, F. Mahmoudi, N. Manglani, and K. Sridhar, *Kaluza Klein gluon + jets associated production at the Large Hadron Collider*, *Phys. Lett.* **B759** (2016) 342–348, [[arXiv:1601.02033](#)].
- [23] J. de Blas, A. Delgado, B. Ostdiek, and A. de la Puente, *LHC Signals of Non-Custodial Warped 5D Models*, *Phys. Rev.* **D86** (2012) 015028, [[arXiv:1206.0699](#)].
- [24] F. Mahmoudi, U. Maitra, N. Manglani, and K. Sridhar, *A Higgs in the Warped Bulk and LHC signals*, *JHEP* **11** (2016) 075, [[arXiv:1608.07407](#)].
- [25] J. A. Cabrer, G. von Gersdorff, and M. Quiros, *Warped Electroweak Breaking Without Custodial Symmetry*, *Phys. Lett.* **B697** (2011) 208–214, [[arXiv:1011.2205](#)].
- [26] A. Alloul, N. D. Christensen, C. Degrande, C. Duhr, and B. Fuks, *FeynRules 2.0 - A complete toolbox for tree-level phenomenology*, *Comput. Phys. Commun.* **185** (2014) 2250–2300, [[arXiv:1310.1921](#)].
- [27] J. Alwall, R. Frederix, S. Frixione, V. Hirschi, F. Maltoni, O. Mattelaer, H. S. Shao, T. Stelzer, P. Torrielli, and M. Zaro, *The automated computation of tree-level and next-to-leading order differential cross sections, and their matching to parton shower simulations*, *JHEP* **07** (2014) 079, [[arXiv:1405.0301](#)].
- [28] R. D. Ball et al., *Parton distributions with LHC data*, *Nucl. Phys.* **B867** (2013) 244–289, [[arXiv:1207.1303](#)].
- [29] T. Sjostrand, S. Mrenna, and P. Z. Skands, *A Brief Introduction to PYTHIA 8.1*, *Comput. Phys. Commun.* **178** (2008) 852–867, [[arXiv:0710.3820](#)].
- [30] M. Cacciari, *FastJet: A Code for fast k_t clustering, and more*, in *Deep inelastic scattering. Proceedings, 14th International Workshop, DIS 2006, Tsukuba, Japan, April 20-24, 2006*, pp. 487–490, 2006. [hep-ph/0607071](#).
- [31] M. Cacciari, G. P. Salam, and G. Soyez, *FastJet User Manual*, *Eur. Phys. J.* **C72** (2012) 1896, [[arXiv:1111.6097](#)].
- [32] Y. L. Dokshitzer, G. D. Leder, S. Moretti, and B. R. Webber, *Better jet clustering algorithms*, *JHEP* **08** (1997) 001, [[hep-ph/9707323](#)].
- [33] S. Bentvelsen and I. Meyer, *The Cambridge jet algorithm: Features and applications*, *Eur. Phys. J.* **C4** (1998) 623–629, [[hep-ph/9803322](#)].
- [34] T. Plehn and M. Spannowsky, *Top Tagging*, *J. Phys.* **G39** (2012) 083001, [[arXiv:1112.4441](#)].
- [35] G. Kasieczka, T. Plehn, T. Schell, T. Strebler, and G. P. Salam, *Resonance Searches with an Updated Top Tagger*, *JHEP* **06** (2015) 203, [[arXiv:1503.05921](#)].
- [36] CMS Collaboration, C. Collaboration, *Identification of b quark jets at the CMS Experiment in the LHC Run 2*, .